coatings

Article

Effect of Cold Rolling on the Microstructural Evolution and Mechanical Properties of Fe-25Mn-3Si-3Al-0.3Nb TWIP Steel

Dejun Li [1,2,*], Jianhua Guo [3], Fei He [3], Yaorong Feng [1,2], Dashan Guo [4], Fengzhang Ren [4], Feng Cao [1,2], Qi Yang [1,2] and Wei Shi [1,2]

1 State Key Laboratory for Performance and Structural Safety for Petroleum Tubular Goods and Equipment Materials, Xi'an 710077, China; fengyr@cnpc.com.cn (Y.F.); caofeng003@cnpc.com.cn (F.C.); yangqi006@cnpc.com.cn (Q.Y.); shiwei006@cnpc.com.cn (W.S.)
2 CNPC Tubular Goods Research Institute, Xi'an 710077, China
3 Engineering Technology Research Institute, PetroChina Southwest Oil & Gas Field Company, Chengdu 618301, China; g_jh@petrochina.com.cn (J.G.); hefei@petrochina.com.cn (F.H.)
4 School of Materials Science and Engineering, Henan University of Science and Technology, Luoyang 471000, China; guodashan1995@163.com (D.G.); renfz@haust.edu.cn (F.R.)
* Correspondence: lidejun352@cnpc.com.cn

Abstract: The microstructural evolution, deformation mechanism and mechanical properties of Fe-25Mn-3Si-3Al-0.3Nb steel in the process of cold rolling were studied by optical microscopy, scanning microscopy, transmission electron microscopy, X-ray diffractometry, tensile testing and microhardness tests. A high-density dislocation structure and a small number of strain-induced twins appeared in the microstructure of the steel at 30% strain. At 50% strain, the strain-induced twins in austenite increased conspicuously, and the lamella thickness of the twins decreased. At 70% strain, the original grains were clearly refined by the micro-shear bands and twinning intersections to form a large number of sub-grains, and some sub-grains were at the nanoscale. The steel still remained a single-phase austenite during cold rolling even if the strain was as high as 70%. The plastic deformation mechanism of the steel was not changed through the addition of 0.3 wt.% Nb, and both dislocation slipping and twinning were still the fundamental plastic deformation mechanisms for the steel. Furthermore, cold rolling led to a drastic rise in the strength and hardness of the steel, but a remarkable decrease in the elongation. The characteristics of micropore aggregation fractures could always be observed on the fracture surface of static tensile specimens with various strains.

Keywords: cold rolling; TWIP steel; Nb-microalloying; twinning; mechanical properties

Citation: Li, D.; Guo, J.; He, F.; Feng, Y.; Guo, D.; Ren, F.; Cao, F.; Yang, Q.; Shi, W. Effect of Cold Rolling on the Microstructural Evolution and Mechanical Properties of Fe-25Mn-3Si-3Al-0.3Nb TWIP Steel. *Coatings* **2022**, *12*, 900. https://doi.org/10.3390/coatings12070900

Academic Editor: Maria Bignozzi

Received: 27 April 2022
Accepted: 17 June 2022
Published: 25 June 2022

1. Introduction

Solid expandable tube (SET) technology represents an innovation for saving the costs of drilling and completing wells that have been used successfully for slim hole casing design and for handling the abnormal pressures encountered downhole during drilling. In addition, this technology has been used to rejuvenate well bores for deepening wells, casing repair and sidetrack drilling for stimulation. The diameter of solid expandable tubes needs to be expanded by ~15% or even by 30% [1,2] downhole through the action of hydraulic pressure or mechanical force, after which the inner diameter of the well bore will be returned to the maximum size. The most essential characteristic of an expandable tube is expandability, which is directly affected by the ductility of the expandable tubular materials. The twinning-induced plasticity (TWIP) effect was reported by Grässel et al. [3], who found that extensive mechanical twins can be aroused in the austenite matrix during the plastic deformation of Fe-25Mn-3Si-3Al steel, and the uniform elongation is three times higher than other steels with high strength and toughness. Researchers have attributed the excellent ductility of the steel to the TWIP effect, because the local plastic deformation is suppressed by the mechanical twins gradually formed during plastic deformation, meaning that TWIP steel has high uniform elongation [4]. TWIP steel is attracting much interest in the research area of advanced steel materials, and is also the focus of many SET researchers.

Fe-25Mn-3Si-3Al TWIP steel, which has excellent ductility, seems to be the ideal raw material for manufacturing SETs [5]. However, the reality is that its low yield strength is the major bottleneck limiting its application in the field of SET, although its other mechanical properties are very suitable for manufacturing expandable casings. Pilot test results have shown that expandable tubes manufactured from Fe-25Mn-3Si-3Al TWIP steel cannot obtain a satisfactory strength after routine expansion. Therefore, an appropriate increase in the yield strength of the steel is important for engineering applications in this field. The yield strength can be increased by methods such as solid solution strengthening, microalloying, grain refinement and work-hardening [4]. In these methods, work-hardening is widely used in modern manufacturing via the facile cold rolling process [6,7]. Up to now, the plastic deformation behavior of TWIP steels during cold rolling has seldom been studied, and the related research has mainly concentrated on austenite stainless steels. The changes in mechanical properties and microstructural evolution of AISI 316L austenitic stainless steel during cold rolling at −15 °C were studied by Eskandari et al. [8]. It was found that the volume fraction of strain-induced martensite in the steel was nearly 70% after cold rolling with 95% reduction, and nano-grained stainless steel can be prepared by rapid annealing at a high temperature. Similar studies have been conducted for AISI 304L stainless steel. The microstructural evolution and mechanical properties of AISI 304L austenitic stainless steel at various strains were investigated at a rolling temperature of −153 °C [9]. The austenite was completely transformed into martensite when the rolling reduction was above 80%, whereas nano-grains appeared in its microstructure and the strength was significantly raised.

In this study, Fe-25Mn-3Si-3Al-0.3Nb TWIP steel was rolled at room temperature, then the microstructural evolution, deformation mechanism and changes in the mechanical properties during cold rolling were investigated in detail. This steel was chosen because it is stronger than Fe-25Mn-3Si-3Al steel, as reported by Grässel et al. It is an improved steel based on Fe-25Mn-3Si-3Al steel through Nb microalloying [10]. To the best of our knowledge, the microstructural evolution mechanism of high-Mn austenitic steels depends on their stacking fault energy (SFE), which is a function of chemical composition and deformation temperature. Huang et al. [11] reported that the trace Nb element added into Fe-25Mn-2Si-2Al steel could promote the mechanism of stain-induced twinning but suppressed the mechanism of martensite phase transformation. Therefore, we wanted to know whether the plastic deformation mechanism of Fe-25Mn-3Si-3Al steel would change when the addition of niobium reached up to 0.3%. After all, strain-induced martensite exhibits higher stress corrosion sensitivity in the oil and gas environment [12]. It is hoped that this research can explore a feasible method for the manufacturing of high-strength TWIP steels and expand their application in the field of SET.

2. Experimental Procedures

The Fe-25Mn-3Si-3Al-0.3Nb steel used in this study was prepared in a vacuum induction melting furnace under an argon atmosphere, and cast into an ingot with a diameter of 150 mm and a height of 450 mm. The ingot was forged to form cube blanks with a side length of 100 mm. The cube blanks were rolled into 20-mm-thick plates, the starting and finishing rolling temperatures were about 1150 °C and 900 °C, respectively. After hot rolling, the hot-rolled sheets were heated at 1050 °C for 120 min and then quenched in water to recover the plasticity and obtain a single-phase austenite microstructure, as shown in Figure 1. The chemical compositions of the experiment steel are listed in Table 1.

Subsequently, sheet samples with three thicknesses of 0.7, 1.0 and 1.7 were cut from the solution-treated hot-rolled plates. Sheet samples were rolled on a self-designed rolling mill with a rolling diameter of 90 mm and a rolling velocity of 0.14 m/s. All the sheet samples were rolled to the same final thickness of 0.5 mm by multi-pass rolling with a 5% reduction per pass. The three thicknesses (0.7, 1.0 and 1.7 mm) were achieved with 7, 17, and 21 rolling passes, respectively. The overall reduction in thickness (i.e., the rolling strains of the three thicknesses) was 30%, 50% and 70%, respectively.

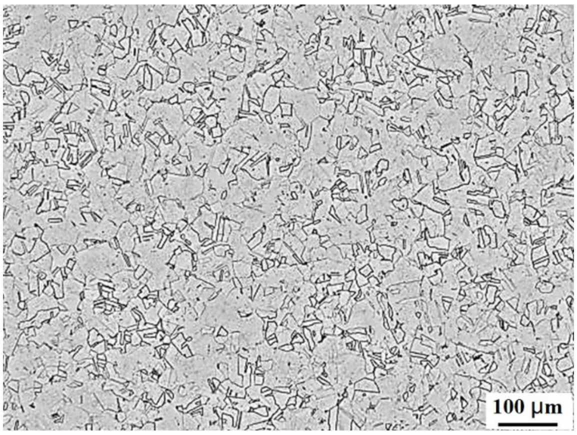

Figure 1. Microstructure of Fe-25Mn-3Si-3Al-0.3Nb steel after solution treatment.

Table 1. Chemical composition of the experimental steels.

Element	C	Mn	Si	Al	Nb	P	S	Fe
[wt.%]	0.08	24.92	2.8	2.82	0.28	0.003	0.001	Bal.

Tensile specimens with a gauge length of 15 mm, width of 3 mm and thickness of 0.2 mm were cut directly from the cold-rolled sheets with different rolling strains along the length direction by wire-electrode cutting. Identical tensile specimens were cut from the solution-treated hot-rolled sheet for comparison. Uniaxial tensile testing was carried out on a CMT-4104 universal testing machine at a tensile rate of 3 mm/min, then the yield strength (0.5% EUL), tensile strength and elongation were measured. The fracture surface morphologies of the tensile specimens were observed with a JSM-7800F scanning electron microscope (JEOL, Tokyo, Japan). The microhardness distributions from surface to center of the steel sheets before and after cold rolling were measured with an MH-3 Vickers microhardness tester (Veiyee, Laizhou, China) with a normal load of 200 g.

The microstructural characteristics of the steel before and after cold rolling were observed using a Zeiss Axio Vert A1 optical microscope and JEOL-2100 transmission electron microscope. The phase compositions of the specimens with various rolling strains were determined by a Bruker D8A X-ray diffractometer (Bruker, Karlsruhe, Germany). The scanning angle range was set from 35° to 95° with a step of 0.02°. The tube voltage and current were 40 kV and 40 mA, respectively.

3. Results

3.1. Microstructure

The XRD spectra of Fe-25Mn-3Si-3Al-0.3Nb steel before and after cold rolling are presented in Figure 2. It can be seen that the steel after treatment with solution had a complete austenitic phase at room temperature; moreover, any new diffraction peaks were not found in the XRD patterns of cold-rolled specimens, indicating that cold rolling deformation did not cause the strain-induced martensite transformation in the steel, even when the deformation reached 70%, although this phenomenon is often found during plastic deformation of austenitic stainless steel.

Figure 3 shows the optical micrographs of Fe-25Mn-3Si-3Al-0.3Nb steel at various rolling strains. It can be seen in Figure 3a that the austenite grains are obviously elongated along the rolling direction at the rolling strain of 30%, but the grain boundaries are still distinguishable. A few slip bands can be observed in some grains, which were also observed for the cold rolling deformation of brass by Kumar et al. [13]. As the rolling strain increases to 50%, the number of slip grains rises fast and some grain boundaries become blurred, and the slip bands within the grain are distributed along the rolling direction. When the rolling strain increases to 70%, the grains are elongated further, and the coarse initial grains are broken and refined through severe plastic deformation, and distributed in fibrous form.

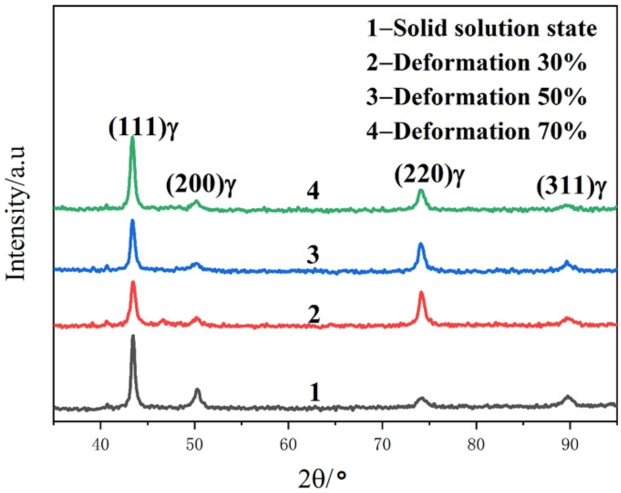

Figure 2. XRD patterns of Fe-25Mn-3Si-3Al-0.3Nb steel before and after cold rolling.

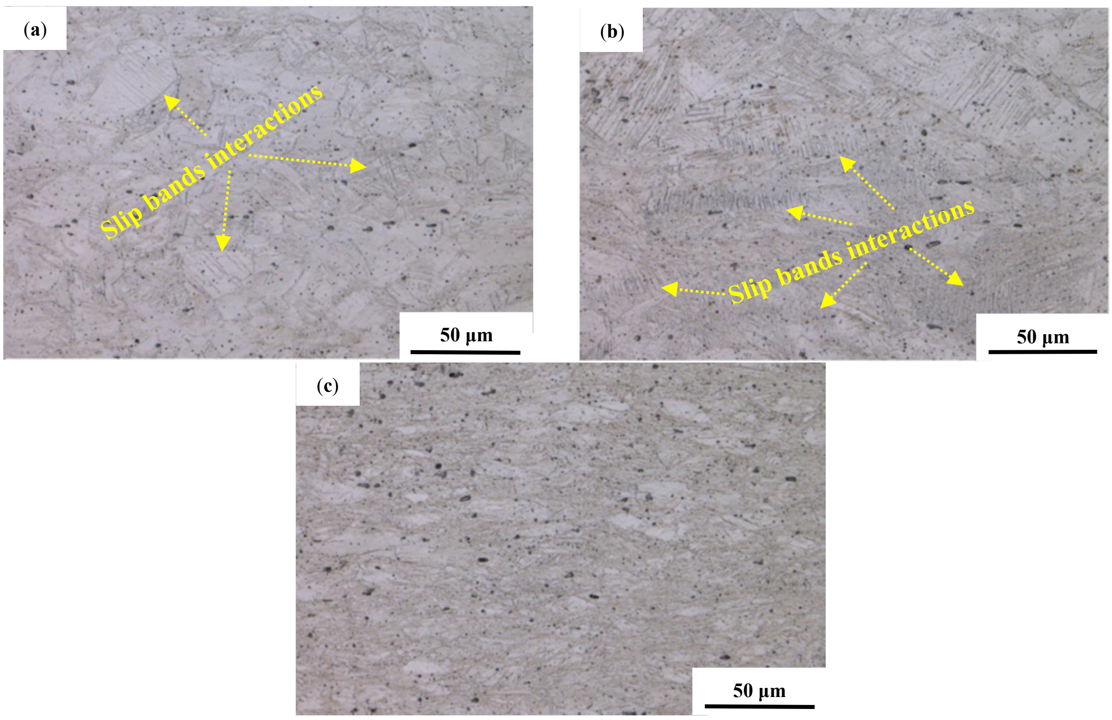

Figure 3. Metallographic structure of Fe-25Mn-3Si-3Al-0.3Nb steel after cold rolling (**a**) after 30% deformation; (**b**) after 50% deformation; (**c**) after 70% deformation.

The TEM images of Fe-25Mn-3Si-3Al-0.3Nb steel after cold rolling are presented in Figure 4. When the rolling strain is 30%, very dense tangled dislocations can be observed in most austenite grains; moreover, a dislocation wall is formed in some grains causing stress concentration in local regions. Furthermore, a small number of mechanical twins can be distinguished in local regions of these grains, as shown in Figure 4a. However, a large number of mechanical twins can be observed in some austenite grains, as shown in Figure 4b. The fine lamellar mechanical twins have a parallel distribution, and high-density dislocations can be found between lamellar twins. Beladi et al. [14] attributed this phenomenon to grain orientation, and they considered that the mechanical twinning propensity in a certain grain is intensely dependent on its crystalline orientation, and different grain orientations result in different twin densities. As the rolling strain increases to 50%, the dislocation density increases further in the grains whose grain orientation is not conducive to twin formation, and the original distorted grains are further refined into massive structures. It is interesting to note that a secondary twinning system is also triggered in grains beside the primary twinning system, as shown in Figure 4c. It can be found in Figure 4d that the thickness of the lamellar twins reduces and the density increases rapidly in grains with favorable orientation for twin growth. Moreover, dislocation wall approximatively normal to the twins' boundaries are formed in the lamellae, and some original grain boundaries can still be observed in the twinning region. Similar phenomena have also been observed by Xiong et al. in the microstructure of Fe-25Cr-20Ni austenitic stainless steel after cryorolling [15]. When the rolling strain increases to 70%, micro-shear bands are formed in the lamellae to adapt to the higher strain, as shown in Figure 4e. The shear effect of the micro-shear bands further refines the grain, and nano-sized twins are formed in local areas. Meanwhile, the original grains are divided by the intersections of twins with different orientations to form a larger number of sub-grains, as shown in Figure 4f. Kusakin et al. believed that appearance of a shear band is a consequence of the saturation of mechanical twins when the rolling strain reaches a certain level [16]. The shear band is an important non-uniform deformation mechanism for metals with a low SFE and usually develops in highly twinned structures characterized by nano-sized twin/matrix lamellae that are formed at the initial stage of deformation [17,18]. Sub-boundaries formed by dislocation walls subdivide the austenite matrix into nanosized blocks with misorientations in the grains with lower twin density [19,20], as shown in Figure 4g,h. Both nano-sized twins and ultrafine sub-grains can be found in the deformed microstructure with 70% strain. Continuous diffraction rings appear in the selected electron diffraction patterns, as shown in Figure 4h, because the original grains are broken into ultrafine sub-grains, and the diffraction pattern of a single crystal is difficult to obtain [21]. This means that the microstructure of Fe-25Mn-3Si-3Al-0.3Nb steel can clearly be refined by cold rolling with high strain, and the microstructure and substructure can be refined to the nanoscale at a rolling strain of 70%.

3.2. Mechanical Properties and Static Tensile Fractography

The stress–strain curves of the testing steel before and after cold rolling are shown in Figure 5. Mechanical properties such as the yield strength, tensile strength and elongation are listed in Table 2. Clearly, the strength of the solution-treated sample is the lowest and the fracture elongation is the highest. As the rolling strain increases to 30%, the elongation decreases from 65.2% to 7.5%, and the yield strength increases to 862 MPa, which is twice that of the solution-treated sample (418 MPa). The strength of steel increases monotonically with the increase in strain, whereas the fracture elongation decreases monotonically. When the rolling strain increases to 70%, the yield strength and ultimate tensile strength increase to 1336 and 1368 MPa, respectively, and the elongation decreases to 6%, which is less than one-tenth of that of the solution-treated sample. The trend of microhardness with the rolling strain is very similar to that of strength. The hardness distributions from the surface to center of the steel sheets with different rolling strains are shown in Figure 6. It can be found that the solution-treated sample exhibits a better hardness uniformity than all the cold-rolled samples, and the cold-rolled sheet at a rolling strain of 30% has the worst hardness uniformity. Moreover, the hardness distribution from surface to center becomes more uniform with the increase in cold rolling strain. This means that a small rolling strain did not generate the same work hardening effect to the sheet center as the sheet surface. Therefore, the hardness in the center of sheet with 30% strain is not conspicuously increased, and the hardness difference between the surface and center reaches 71 HV. The hardness difference between the surface and center gradually narrows with the increase of rolling strain, and the hardness difference is only 31 HV as the rolling strain reaches 70%.

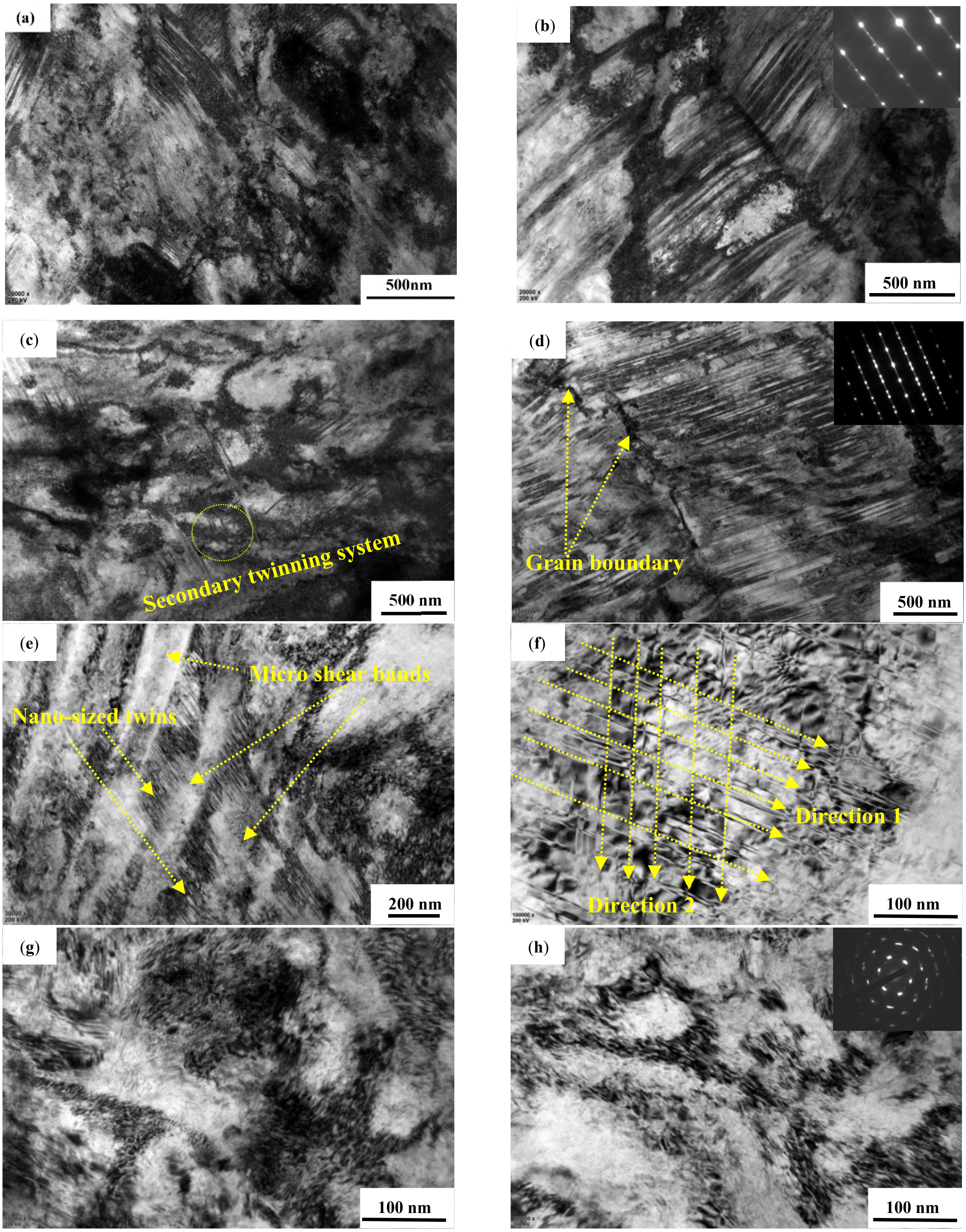

Figure 4. TEM images of Fe-25Mn-3Si-3Al-0.3Nb steel after cold rolling: (**a**,**b**) after 30% deformation; (**c**,**d**) after 50% deformation; (**e**–**h**) after 70% deformation.

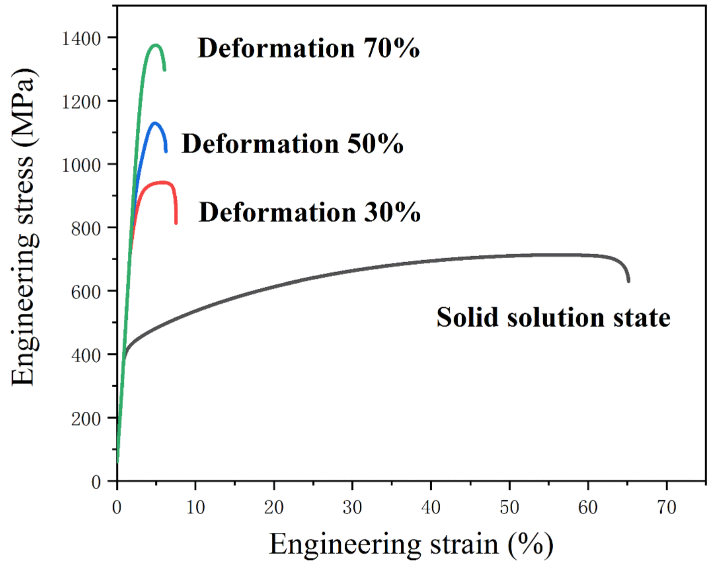

Figure 5. Engineering stress–strain curves of Fe-25Mn-3Si-3Al-0.3Nb steel before and after cold rolling.

Table 2. Mechanical properties of Fe-25Mn-3Si-3Al-0.3Nb steel before and after cold rolling.

Rolling Strain	Yield Strength MPa	Tensile Strength MPa	Elongation %
0%	418	713	65.2
30%	862	942	9.1
50%	904	1128	6.2
70%	1336	1368	6.0

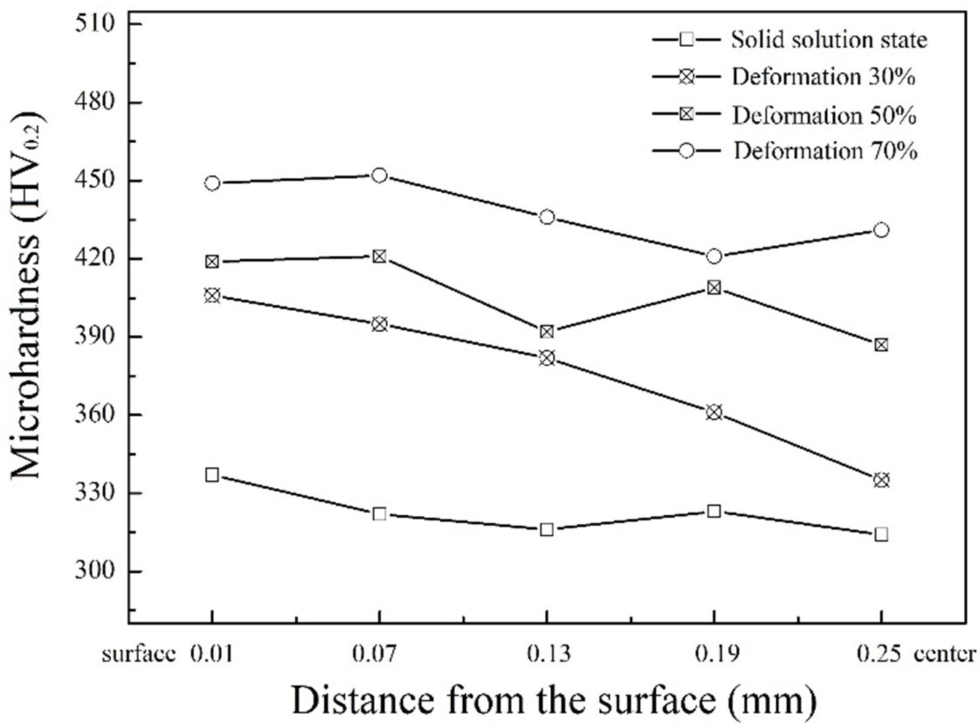

Figure 6. Microhardness distributions along the thickness direction of cold-rolled sheets with different strains.

The fracture morphologies of the static tensile specimens with various strains are shown in Figure 7. The fracture surfaces of the tensile specimens in both the solid solution and cold rolling states present characteristics of microporous aggregation fractures. Before rolling deformation, the solution-treated steel demonstrates excellent plasticity and toughness. Moreover, the typical ductile fracture characteristics are present on the fracture surface, and the dimples are large and deep. As the rolling strain increases to 30% or even 50%, the dimples on the fractures of tensile specimens are flattened and become smaller than those of the solution-treated specimen. When the rolling strain of the tensile specimen reaches 70%, the depth of the dimples on the fracture becomes shallower and smaller. Although cold rolling causes obvious changes in the mechanical properties of the testing steel, micropore aggregation fracture is still the main fracture mechanism, and few features of cleavage fracture can be distinguished on the fracture surface of tensile specimens at various rolling strains.

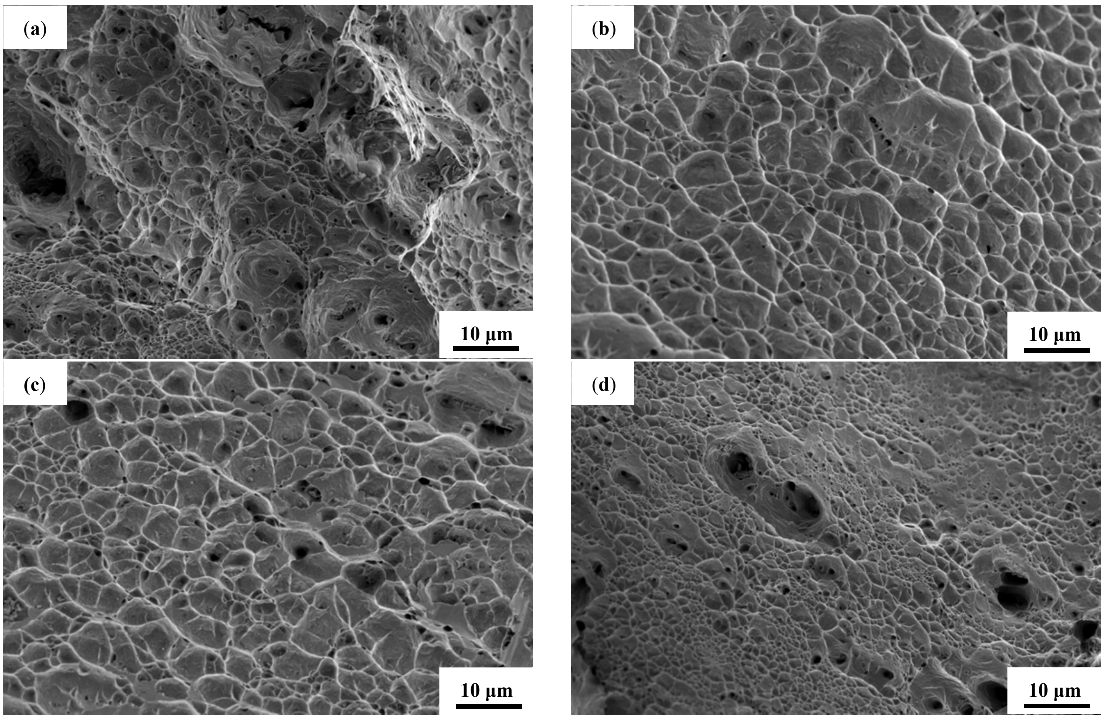

Figure 7. Fracture surface morphology of Fe-25Mn-3Si-3Al-0.3Nb steel before and after cold rolling (**a**) solid solution; (**b**) after 30% deformation; (**c**) after 50% deformation; (**d**) after 70% deformation.

4. Discussion

The tensile test results showed that the single-phase austenite structure has good strength and excellent plasticity in the Fe-25Mn-3Si-3Al-0.3Nb steel before cold rolling. It is generally believed that in high Mn austenitic steels, the TWIP mechanism is more conducive to improvements in the uniform plasticity of the steels than a single dislocation slipping mechanism because the local plastic deformation is depressed by the strain-induced twins. The mechanical twin nucleation must be conducted with the help of stress concentrations caused by a pile-up of dislocations to conquer the critical resolved shear stress $\tau^{\text{C-twin}}$. Moreover, there also exists a competition between TWIP mechanism and dislocation slipping. The SFE of austenite matrix is the decisive factor, and a high SFE is not conducive to the occurrence of mechanical twins. Equation (1) is used to calculate the SFE of austenitic stainless steels [22]; however, the SFE of high Mn austenitic steels is usually calculated based on thermodynamic theory, and there is no similar general calculation formula for high Mn austenitic steels at present.

$$\mathrm{SFE}(\mathrm{mJm}^{-2}) = -7.1 + 2.8(\%\mathrm{Ni}) + 0.49(\%\mathrm{Cr}) + 2.0(\%\mathrm{Mo}) - 2.0(\%\mathrm{Si}) + 0.75(\%\mathrm{Mn}) - 5.7(\%\mathrm{C}) \quad (1)$$

Therefore, dislocation slipping and twinning were the main plastic deformation mechanisms of the steel at the early stages of deformation [23]. The dislocations within the grains proliferated greatly, and deformation twins can be observed in some well-oriented grains. A large number of fixed dislocations formed because of the dislocation/dislocation and dislocation/twin interactions, which act as barriers to mobile dislocation and significantly increases the hardening of the dislocation [24,25]. Densely accumulated dislocation forms in the grains, the strength and hardness of the steel are greatly improved, and the ductility of the steel is severely reduced. With an increase in the rolling strain, more and more mechanical twins are formed in the grains, and the mass of the twins' boundaries effectively shorten the average free path of dislocation movement, becoming a strong obstacle to dislocation [26], and the interaction between the dislocations and twins is clearly enhanced. As a consequence, the strength and hardness of the steel are improved further, whereas the elongation decreases.

With a continuous increase in the rolling strain, micro-shear bands can be observed in the microstructure, meanwhile a large number of dense deformation twins can be observed near the formation area of the shear bands, and there are broken grains with a certain orientation inside the shear bands. The shear band is formed in the region containing dense deformation twins and lamellar matrix by cutting off the continuous fine twin structure, in other words, the shear band is formed by mutual shearing between twins and matrix inside grains. With a further increase in rolling strain, the increase of shear band results in a reduction of the volume fraction of twins in the saturated state meanwhile the grains are completely broken. Finally, the ultrafine sub-grains are formed in the microstructure and the density of the mechanical twins in the grains decreases greatly. Etemad et al. [27] reported a similar phenomenon in the process of accumulative roll bonding of Fe-31Mn-3Al-3Si TWIP steel at room temperature, and they attribute this phenomenon to the inverse grain size effect of mechanical twins. The formation of ultrafine sub-grains leads to a continuous increase in the hardness and strength of the steel, and a sharp decrease in the twinning density leads to a further decrease in the steel's plasticity.

The results show that twinning is still the main deformation mechanism of the experimental steel during cold rolling, and the strain-induced martensite transformation mechanism which is often observed in the plasticity deformation of austenite stainless steel does not occur, even when the cold rolling strain reached as high as 70%. In other words, the addition of 0.3 wt.% Nb does not cause significant changes in the SFE of Fe-25Mn-3Si-3Al steel. It can be known from [28] that the SFE value is a determining factor of the plasticity mechanism of Fe–Mn–C alloy, $\gamma \rightarrow \varepsilon$ transformation is the dominant mechanism when SFE < 18 mJ·m^{-2}, and twinning is the main deformation mechanism when the SFE value ranges from 12 to 35 mJ·m^{-2}. Huang et al. [11] reported that the SFE of Fe-23Mn-2Si-2Al steel increased due to the addition of 0.017 wt.% Nb, $\gamma \rightarrow \varepsilon$ transformation was inhibited, and the strength of the steel decreased but its plasticity improved. They believed that the addition of 0.017 wt.% Nb changes the plastic deformation mechanism of the Fe-23Mn-2Si-2Al steel. These conflicting results may involve the existence of a form of niobium and carbon atoms in the austenite. It is known from [29] that the addition of niobium atoms into austenitic stainless steels exist preferentially in the steels as carbides or nitrides. Thus, the content of Nb must be more than eight times the total content of C and N elements to precipitate all the interstitial atoms from the steel when the total content of C and N > 0.017 wt.%.

Almost all the interstitial atoms in the Fe-25Mn-3Si-3Al TWIP steel combine with Nb atoms to form niobium carbide precipitates through the addition of 0.3 wt.% Nb. In Figure 8, a large amount of precipitates consisting mainly of NbC carbide can be observed in the austenite matrix. It is well known that the strengthening effect of precipitates depends on their volume fraction and dispersion. In Huang's paper, the steel could not be strengthened due to the ultra-low carbon content of the experimental steel and trace additions of niobium. Moreover, carbon atoms precipitate from the austenite through the addition of Nb, which results in a lower solid solubility of the carbon atoms in the austenite matrix. As noted, the SFE is mainly influenced by chemical compositions of austenite matrix. Therefore, the SFE of the austenite matrix of the Fe-23Mn-2Si-2Al steel is changed, and then the $\gamma \rightarrow \varepsilon$ transformation is inhibited while the twin mechanism is stimulated.

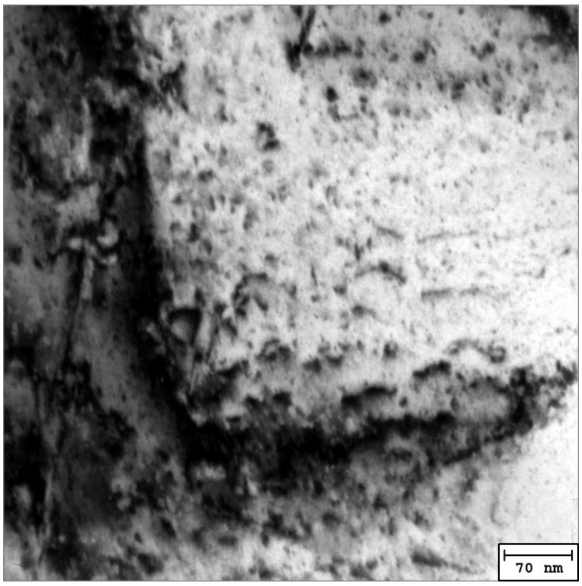

Figure 8. Precipitated particles in the Fe-25Mn-3Si-3Al-0.3Nb steel after solution treatment.

In this paper, the carbon content of Fe-25Mn-3Si-3Al steel was deliberately raised to 0.1 wt.% to offset the carbon loss derived from precipitation and to avoid the obvious change in the SFE of the austenite matrix. The twinning mechanism still plays a key role during plastic deformation at room temperature, in addition to dislocation slipping, although the Nb content of the steel studied in this paper was as high as 0.30 wt.%. In other words, the SFE of austenite matrix of Fe-25Mn-3Si-3Al-0.3Nb steel is still within the range of TWIP mechanism.

5. Conclusions

The effects of cold rolling on the microstructural and mechanical properties of Fe-25Mn-3Si-3Al-0.3Nb steel have been investigated systematically in this paper. Several conclusions are listed as follows:

(1) In addition to dislocation slipping, the twinning mechanism still plays a key role during plastic deformation of Fe-25Mn-3Si-3Al-0.3Nb steel at room temperature. The addition of niobium will not significantly change the plasticity mechanism of Fe-25Mn-3Si-3Al steel given that the existing forms and relative content of carbon and niobium in the steel are well controlled.

(2) As the cold rolling strain increases from 30% to 70%, the Fe-25Mn-3Si-3Al-0.3Nb steel undergoes a microstructural evolution process of generating dense dislocations, deformation twins, shear bands and an ultrafine sub-grain structure in that order.

(3) The strength and hardness of Fe-25Mn-3Si-3Al-0.3Nb steel increases clearly with the increasing of rolling strain, and the ductility decreases greatly, but the fracture mechanism of the static tensile specimens with different rolling strains is always microporous aggregate fracturing.

Author Contributions: Conceptualization, D.L. and J.G.; methodology, F.R.; validation, F.H. and F.R.; formal analysis, D.G.; investigation, D.G.; data curation, F.C.; writing—original draft preparation, D.L.; writing—review and editing, Q.Y.; visualization, W.S.; supervision, Y.F.; project administration, D.L.; funding acquisition, D.G. All authors have read and agreed to the published version of the manuscript.

Funding: This work was supported by Basic Research and Strategic Reserve Technology Research of PetroChina Company Limited (No. 2018Z-03), the Scientific Research and Technology Development Project of PetroChina Company Limited (No. 2017F–19) and the Special Support Program for High Level Talents of Shaanxi Province (No. 00439).

Institutional Review Board Statement: Not applicable.

Informed Consent Statement: Not applicable.

Data Availability Statement: Not applicable.

Conflicts of Interest: The authors declare no conflict of interest.

References

1. Seibi, A.C.; Al-Hiddabi, S.; Pervez, T. Structural behavior of a solid tubular undef large radial plastic expansion. *J. Energy Resour. Technol.* **2005**, *127*, 323–327. [CrossRef]
2. Pervez, T.; Qamar, S.Z.; Seibi, A.C.; Al-Jahwari, F.K. Use of SET in cased and open holes: Comparison between aluminum and steel. *Mater. Des.* **2008**, *29*, 811–817. [CrossRef]
3. Grässel, O.; Krüger, L.; Frommeyer, G.; Meyer, L.W. High strength Fe-Mn-(Al, Si) TRIP/TWIP steels development-properties-application. *Int. J. Plast.* **2000**, *16*, 1391–1409. [CrossRef]
4. Bouaziz, O.; Allain, S.; Scott, C.P.; Cugy, P.; Barbier, D. High manganese austenitic twinning induced plasticity steels: A review of the microstructure properties relationships. *Curr. Opin. Solid State Mater. Sci.* **2011**, *15*, 141–168. [CrossRef]
5. Park, G.; Jeong, S.; Kang, H.; Lee, C. Improvement of circumferential ductility by reducing discontinuities in a high-Mn TWIP steel weldment. *Mater. Charact.* **2018**, *139*, 293–302. [CrossRef]
6. Huang, J.X.; Ye, X.N.; Xu, Z. Effect of cold rolling on microstructure and mechanical properties of AISI 301LN metastable austenitic stainless steel. *J. Iron Steel Res. Int.* **2012**, *19*, 59–63. [CrossRef]
7. Morikawa, T.; Higashida, K. The role of deformation twinning in the formation of a fine-grained structure in cold-rolled 310 steel. *J. Mater. Sci.* **2006**, *41*, 2581–2585. [CrossRef]
8. Eskandari, M.; Najafizadeh, A.; Kermanpur, A. Effect of strain-induced martensite on the formation of nanocrystalline 316L stainless steel after cold rolling and annealing. *Mater. Sci. Eng. A* **2009**, *519*, 46–50. [CrossRef]
9. Roy, B.; Kumar, R.; Das, J. Effect of cryorolling on the microstructure and tensile properties of bulk nano-austenitic stainless steel. *Mater. Sci. Eng. A* **2015**, *631*, 241–247. [CrossRef]
10. Li, D.J.; Feng, Y.R.; Song, S.Y.; Liu, Q.; Bai, Q.; Wu, G.; Lv, N.; Ren, F.Z. Influence of Nb-microalloying on microstructure and mechanical properties of Fe-25Mn-3Si-3Al TWIP steel. *Mater. Des.* **2015**, *84*, 238–244. [CrossRef]
11. Huang, B.X.; Wang, X.D.; Rong, Y.H.; Wang, L.; Jin, L. Mechanical behavior and martensitic transformation of an Fe-Mn-Si-Al-Nb alloy. *Mater. Sci. Eng. A* **2006**, *438–440*, 306–311. [CrossRef]
12. Karlsen, W.; Dyck, S.V. The effect of prior cold-work on the deformation behaviour of neutron irradiated AISI 304 austenitic stainless steel. *J. Nucl. Mater.* **2010**, *406*, 127–137. [CrossRef]
13. Kumar, R.; Dasharath, S.M.; Kang, P.C.; Koch, C.C.; Mula, S. Enhancement of mechanical properties of low stacking fault energy brass processed by cryorolling followed by short-annealing. *Mater. Des.* **2015**, *67*, 637–643. [CrossRef]
14. Beladi, H.; Timokhina, I.B.; Estrin, Y.; Kim, J.; De Cooman, B.C.; Kim, S.K. Orientation dependence of twinning and strain hardening behaviour of a high manganese twinning induced plasticity steel with polycrystalline structure. *Acta Mater.* **2011**, *59*, 7787–7799. [CrossRef]
15. Xiong, Y.; He, T.T.; Wang, J.B.; Lu, Y.; Chen, L.F.; Ren, F.Z.; Liu, Y.L.; Volinsky, A.A. Cryorolling effect on microstructure and mechanical properties of Fe-25Cr-20Ni austenitic stainless steel. *Mater. Des.* **2015**, *88*, 398–405. [CrossRef]
16. Kusakin, P.; Belyakov, A.; Haase, C.; Kaibyshev, R.; Molodov, D.A. Microstructure evolution and strengthening mechanisms of Fe-23Mn-0.3C-1.5Al TWIP steel during cold rolling. *Mater. Sci. Eng. A* **2014**, *617*, 52–60. [CrossRef]
17. Lu, K.; Hansen, N. Structural refinement and deformation mechanisms in nanostructured metals. *Scr. Mater.* **2009**, *60*, 1033–1038. [CrossRef]
18. Hong, C.S.; Tao, N.R.; Huang, X.; Lu, K. Nucleation and thickening of shear bands in nano-scale twin/matrix lamellae of a Cu-Al alloy processed by dynamic plastic deformation. *Acta Mater.* **2010**, *58*, 3103–3116. [CrossRef]
19. Tao, N.R.; Zhang, H.W.; Lu, H.; Lu, K. Development of nanostructures in metallic materials with low stacking fault energies during surface mechanical attrition treatment (SMAT). *Mater. Trans.* **2003**, *44*, 1919–1925. [CrossRef]
20. Tao, N.R.; Wu, X.L.; Sui, M.L.; Lu, J.; Lu, K. Grain refinement at the nanoscale via mechanical twinning and dislocation interaction in a nickel-based alloy. *J. Mater. Res.* **2004**, *19*, 1623–1629. [CrossRef]
21. Yu, W.X.; Liu, B.X.; He, J.N.; Chen, C.X.; Fang, W.; Yin, F.X. Microstructure characteristics, strengthening and toughening mechanism of rolled and aged multilayer TWIP/maraging steels. *Mater. Sci. Eng. A* **2019**, *767*, 138426. [CrossRef]
22. Moshtaghi, M.; Safyari, M. Effect of work-hardening mechanisms in asymmetrically cyclic-loaded austenitic stainless steels on low-cycle and high-cycle fatigue behavior. *Steel Res. Int.* **2021**, *92*, 2000242. [CrossRef]
23. Dini, G.; Najafizadeh, A.; Ueji, R.; Monir-Vaghefi, S.M. Tensile deformation behavior of high manganese austenitic steel: The role of grain size. *Mater. Des.* **2010**, *31*, 3395–3402. [CrossRef]

24. Gutierrez-Urrutia, I.; Raabe, D. Multistage strain hardening through dislocation substructure and twinning in a high strength and ductile weight-reduced Fe-Mn-Al-C steel. *Acta Mater.* **2012**, *60*, 5791–5802. [CrossRef]
25. Steinmetz, D.R.; Japel, T.; Wietbrock, B.; Eisenlohr, P.; Gutierrez-Urrutia, I.; Saeed-Akbari, A.; Hickel, T.; Roters, F.; Raabe, D. Revealing the strain-hardening behavior of twinning-induced plasticity steels: Theory, simulations, experiments. *Acta Mater.* **2013**, *61*, 494–510. [CrossRef]
26. Barbier, D.; Gey, N.; Allain, S.; Bozzolo, N.; Humbert, M. Analysis of the tensile behavior of a TWIP steel based on the texture and microstructure evolutions. *Mater. Sci. Eng. A* **2009**, *500*, 196–206. [CrossRef]
27. Etemad, A.; Dini, G.; Schwarz, S. Accumulative roll bonding (ARB)-processed high-manganese twinning induced plasticity (TWIP) steel with extraordinary strength and reasonable ductility. *Mater. Sci. Eng. A* **2019**, *742*, 27–32. [CrossRef]
28. Allain, S.; Chateau, J.P.; Bouaziz, O. Correlations between the calculated stacking fault energy and the plasticity mechanism in Fe–Mn–C alloy. *Mater. Sci. Eng. A* **2004**, *387*, 158–162. [CrossRef]
29. Meng, F.M.; Fu, J.Y. *Modern Stainless Steel Containing Niobium*, 1st ed.; Metallurgy Industry Press: Beijing, China, 2004. (In Chinese)